Optical properties of vanadium ions in ZnSe

1992 J. Phys.: Condens. Matter 4 8253

(http://iopscience.iop.org/0953-8984/4/42/014)

J. Phys.: Condens. Matter 4 (1992) 8253–8266. Printed in the UK

Optical properties of vanadium ions in ZnSe

G Goetz†, U W Pohl‡ and H-J Schulz†

† Fritz-Haber-Institut der Max-Planck-Gesellschaft, Faradayweg 4-6, D-1000 Berlin 33, Federal Republic of Germany

‡ Institut für Festkörperphysik der Technischen Universität Berlin, Hardenbergstraße 36, D-1000 Berlin 12, Federal Republic of Germany

Received 27 November 1991, in final form 28 April 1992

Abstract. The photoluminescence of intentionally vanadium-doped ZnSe crystals displays at low temperatures ($T \approx 4$ K) the emission of the V^{3+} (d^2), V^{2+} (d^3) and V^+ (d^4) ions with different no-phonon structures at 5440, 4740 and 3640 cm^{-1}, respectively. The excitation spectra of the V^{3+} and V^{2+} luminescence bands are investigated separately and exhibit structures of the respective spin-allowed as well as spin-forbidden internal transitions, which are largely in accordance with those of ZnS:V. The corresponding energy levels are approximated in a computation following the Tanabe–Sugano scheme. Furthermore, charge transfer processes at the luminescent centres are manifest in excitation, stimulation and transmission spectra. The vanadium ion proves to be an amphoteric impurity. Commencing from V^{2+}, the state with neutral effective charge, light-induced transitions of donor and acceptor type are disclosed: $V^{2+} \leftrightarrow V^{3+} + e^-_{CB}$ and $V^{2+} \leftrightarrow V^+ + e^+_{VB}$.

1. Introduction

The optical properties of vanadium-activated II–VI compounds have been investigated for a long time. For ZnS, ZnSe, CdS and CdSe, both in emission (Avinor and Meijer 1960) and excitation (Meijer and Avinor 1960), characteristic broad bands were recorded at 12 900 cm^{-1}, 8900 cm^{-1} and 5000 cm^{-1}, and later attributed to transitions into the states $^3T_1(P)$, $^3T_1(F)$ and $^3T_2(F)$, respectively, of the V^{3+} ($3d^2$) centre in a tetrahedral crystal field (Allen 1963). Better-resolved emission and excitation spectra of CdS:V crystals were also interpreted under the assumption of V^{3+} transitions (Buhmann *et al* 1979). In some cases, however, absorption and emission structures of V-doped II–VI semiconductors were explained by the presence of divalent $V^{2+}(3d^3)$ ions (Wray and Allen 1971, Le Manh and Baranowski 1977). More recent results with ZnS:V crystals demonstrate the occurrence of several emission and corresponding excitation bands which must be assigned to different vanadium charge states appearing simultaneously (Biernacki *et al* 1988, Schulz *et al* 1990). Distinct optical bands could be firmly attributed to intra-d-shell transitions of V^{3+} (d^2) and V^{2+} (d^3) and, tentatively, also to V^+ (d^4).

As demonstrated in the present study, the three mentioned charge states of the V ion can also occur in ZnSe crystals. While the general features of the V (d^n) transitions show strong similarities to the spectra in ZnS, considerable differences have been found in the fine structure. In addition to the crystal-field transitions an analysis of charge transfer processes is presented.

0953-8984/92/428253+14$04.50

2. Luminescence spectra

ZnSe crystals with different concentrations of vanadium were studied. In addition to some crystals accidentally contaminated by vanadium, several intentionally vanadium-doped samples were grown from the melt by the high-pressure Bridgman method. The presented spectra were recorded from specimens with nominal vanadium doping of 100 ppm, 300 ppm and 3000 ppm (numbers 5019, 5021, 5022, respectively).

The emission measurements were carried out by means of 1-m grating spectrometer (Jarrell–Ash, grating blazed at 1.6 μm). The crystals were cooled in a He bath cryostat. The luminescence was excited by a YAG:Nd laser (9400 cm^{-1} line) or by a high-pressure Xe lamp and detected by a cooled ($T \approx 240$ K) PbS photoresistor. The emission spectra have been corrected for grating efficiency variations and for the spectral response of the PbS detector.

At all investigated vanadium doping levels, three structured luminescence bands centred near 5100 cm^{-1}, 4350 cm^{-1} and 3450 cm^{-1} appear simultaneously. Each emission consists of narrow no-phonon lines (NPL) at the high-energy onset followed by a broad phonon-assisted band at lower energy. All the three emissions show different excitation behaviour indicating their different origin. Spectra with similar properties have been reported for vanadium-doped ZnS crystals, where three luminescence bands centred at 5550 cm^{-1}, 4800 cm^{-1} and 3750 cm^{-1} were detected (Biernacki *et al* 1988, Schulz *et al* 1990).

The shape and detailed structures of the 5100 cm^{-1} luminescence in ZnSe (figure 1) resemble the course of the well known emission bands in InP:V, GaAs:V and the high-energy emission band in ZnS:V. They were ascribed to the $^3T_2(F) \rightarrow {}^3A_2(F)$ transition of the V^{3+} ion. This assignment was confirmed in the III–V semiconductors by means of Zeeman- and piezo-spectroscopy (Skolnick *et al* 1983, Armelles *et al* 1984, Nash *et al* 1984, Aszódi and Kaufmann 1985). Moreover, EPR studies with ZnSe:V (Dieleman 1967) proved that V^{3+} was incorporated substitutionally on a Zn lattice site. Therefore, the interpretation in terms of an internal transition of the V^{3+} ion is adopted for the luminescence of ZnSe:V. The phonon sidebands of the V^{3+} emission are dominated by coupling to optical modes. The most prominent satellite structure at a distance of 196 cm^{-1} from the NPL is, as in the aforementioned V^{3+} systems, a slightly reduced TO phonon of the host lattice. The sharp line at 5036 cm^{-1} on the low-energy tail of the V^{3+} emission band is assigned to traces of Ni^{3+} (Goetz and Schulz 1992).

At elevated temperatures, a considerably weaker 'hot' line appears at 5451 cm^{-1} on the high-energy side of the no-phonon line at 5440 cm^{-1}. Thermalization of the participating energy levels was realized by an enhancement of the laser power during excitation ($P = 2$ W). The distance between the two lines $\Delta\bar{\nu} = 11$ cm^{-1} reflects a twofold splitting of the excited state and is also observed with ZnS:V^{3+} ($\Delta\bar{\nu} = 11$ cm^{-1}, Biernacki *et al* (1988)) and GaAs:V^{3+} ($\Delta\bar{\nu} = 10$ cm^{-1}, Aszódi and Kaufmann (1985)). Under the influence of spin–orbit coupling the excited $^3T_2(F)$ term is split according to $\Gamma_5 \otimes \Gamma_4$ into the four components Γ_4, Γ_3, Γ_5 and Γ_2, as indicated in the insert of figure 1. The magnitude of the splitting between these spin–orbit levels depends on the strength of a Jahn–Teller interaction which affects the excited state (Aszódi and Kaufmann 1985). With increasing Jahn–Teller coupling, the four electronic levels merge into a sixfold ($\Gamma_4 + \Gamma_5$) and a lower lying threefold degenerate vibronic level ($\Gamma_2 + \Gamma_3$), jointly forming the initial states of the observed 'NPL' transitions.

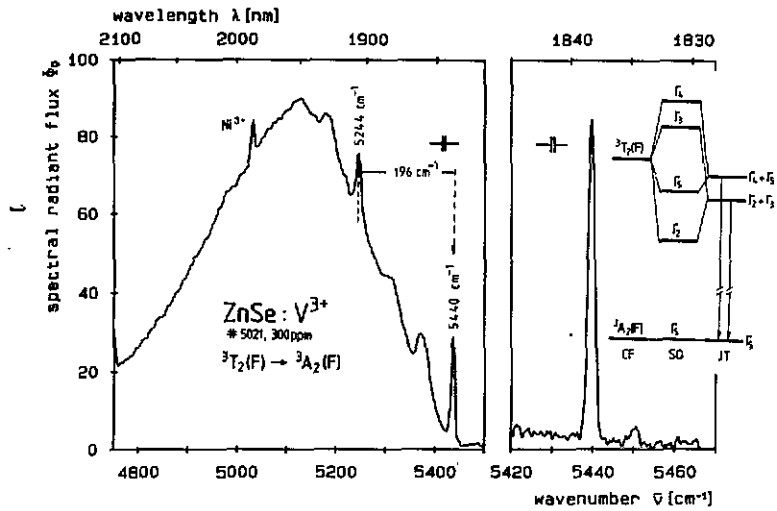

Figure 1. Left: emission spectrum of ZnSe:V^{3+} at $T \approx 4$ K (crystal number 5021), right: thermalization of the no-phonon transitions at $T > 4$ K; corrected spectra. Excitation: YAG:Nd-laser, $\bar{\nu} \approx 9400$ cm^{-1}. Insert: splitting of the lowest many-electron multiplets of the d^2 configuration; cf text.

The emission band centred near 4350 cm^{-1} (figure 2) displays six no-phonon lines at 4755, 4751, 4743, 4737, 4723 and 4718 cm^{-1} (the weak 'line' at 4729 cm^{-1} is not reproducible and is ascribed to noise). In analogy to ZnS, this luminescence is attributed to the $^4T_2(F) \rightarrow {}^4T_1(F)$ transition of the V^{2+} (d^3) ion. In ZnS, however, the V^{2+} emission just shows a no-phonon doublet.

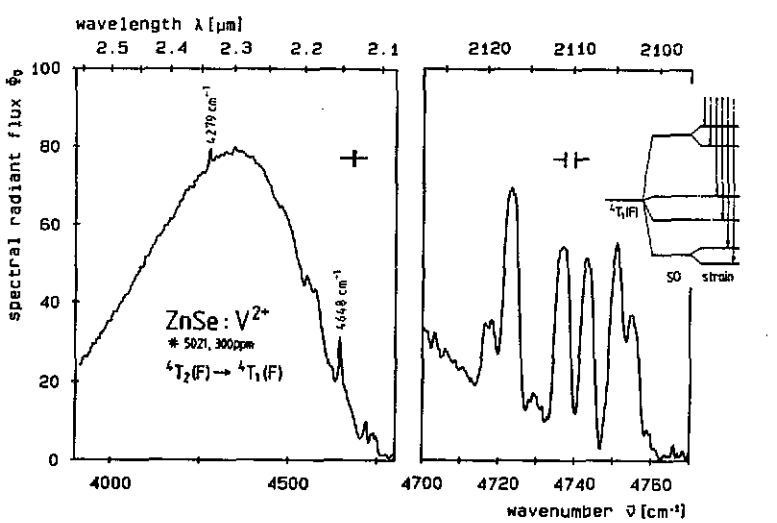

Figure 2. Left: emission spectrum of ZnSe:V^{2+} at $T \approx 4$ K (crystal number 5021), right: no-phonon lines of ZnSe:V^{2+} at increased resolution; corrected spectra. Excitation range: 16 500 cm^{-1} $\leqslant \bar{\nu} \leqslant$ 27 000 cm^{-1}. Insert: schematic splitting of the $^4T_1(F)$ ground state of the d^3 configuration; for discussion see text.

The sixfold splitting of the no-phonon emission in ZnSe:V^{2+} is observed at very

low temperature and must thus be related to splitting of the ground state. In principle, the V^{2+} ground state might be the high-spin $^4T_1(F)$ or the low-spin $^2E(G)$ state. A low-spin model for V^{2+} was recently constructed theoretically (Katayama-Yoshida and Zunger 1986, Caldas *et al* 1986) and the experiments tended to support the prediction for GaAs:V (Hennel *et al* 1987). For ZnSe:V, the observed sixfold splitting (cf figure 2) cannot result from a ^2E ground state but from a high-spin state $^4T_1$, as realized in ZnS:V (Biernacki *et al* 1988).

Considering spin–orbit interaction with $S = 3/2$, the components of the $^4T_1(F)$ ground state and those of $^4T_2(F)$ transform according to $\Gamma_i \otimes \Gamma_8 = \Gamma_6 + \Gamma_7 + 2\Gamma_8$, with $i = 4, 5$. Whereas Γ_6 and Γ_7 are two-dimensional representations of the double group $\overline{T}_d$, Γ_8 is four-dimensional. The fourfold degeneracy of Γ_8 levels can be lifted by electric fields, producing two further levels Γ_6 and Γ_7, each of twofold degeneracy. A decomposition of the Γ_8 levels resulting in a sixfold splitting of a $^4T_1$ level has been stated recently in the case of the luminescent $^4T_1(G)$ level of the Mn^{2+} ion in stacking-faulted ZnS (Pohl *et al* 1990). Presence of stacking faults is, however, not plausible for ZnSe which is preferentially of cubic structure.

As no thermalization effects occur for the no-phonon lines, the spin–orbit splitting of the excited $^4T_2(F)$ term cannot be specified. Therefore, the lowest excited level is assumed to be Γ_8–$^4T_2(F)$ as in ZnS:V^{2+} (Biernacki *et al* 1988), and selection rules are still considered for electric-dipole transitions in $\overline{T}_d$. The six no-phonon lines can thus tentatively be interpreted as transitions into spin–orbit levels of the $^4T_1(F)$ ground state whose Γ_8 components are split into Γ_6 and Γ_7 states, as indicated in the insert of figure 2. The reason for this additional splitting is not yet clear. For a precise assignment of the structures, further Zeeman, uniaxial stress or EPR experiments could yield useful information.

As the observed total spin–orbit splitting of the $^4T_1(F)$ ground state is smaller than for the free ion, the orbital momentum is reduced by dynamic Jahn–Teller interaction. Similar to the case of the $^3T_2(F)$ level of V^{3+} mentioned above, a sufficiently strong Jahn–Teller coupling would compress the four spin–orbital components of the $^4T_1(F)$ term into two levels originating from the representations $(\Gamma_6 + \Gamma_8)$ and $(\Gamma_7 + \Gamma_8)$, each of sixfold degeneracy (Koidl 1976). The coupling strength of the V^{2+} ion turns out to be considerably lower in ZnSe than in ZnS, where only a doublet is observed (Biernacki *et al* 1988).

The ratio of spectral intensities in the V^{3+} and V^{2+} emission bands depends on the excitation conditions. Whereas V^{2+} luminescence is preferred under irradiation in the high-energy regime ($16\,500\ cm^{-1} \leqslant \bar{\nu} \leqslant 27\,000\ cm^{-1}$), both emissions are almost of equal strength at an excitation energy of $\bar{\nu} \approx 9400\ cm^{-1}$ (YAG:Nd). In this case, the maximum of the V^{2+} band shifts towards higher energy by about 70 cm^{-1} due to the higher V^{3+} 'underground'. Moreover, different excitation conditions affect the vibronic structures. Marked changes occur under the laser irradiation in the region of the first prominent satellite at 4648 cm^{-1}. While this line is less distinct than under broad-band excitation with the Xe lamp, a strong shoulder additionally appears on its high-energy slope. These changes of the emission band structure cannot merely be explained by a possible temperature increase or by an underground raised by the tail of the V^{3+} emission. They are thought to result from an excitation-induced change of the phonon coupling. The distance between this first satellite and the no-phonon lines near 4720 cm^{-1} is approximately 72 cm^{-1}, suggesting the coupling of a resonant TA mode. Structures at 4578, 4552 and 4480 cm^{-1} can be described by coupling of LA and LO phonons of the ZnSe host lattice (LA $\approx$ 160 cm^{-1} and LO $\approx$ 255 cm^{-1},

cf Mitra (1966), Irwin and La Combe (1972)).

While the line at 5036 cm^{-1} on the V^{3+} emission spectrum is ascribed to Ni^{3+}, no interpretation can be given for the weak structure occurring in all three specimens at 4279 cm^{-1} on the low-energy tail of the V^{2+} emission.

At lower energy, a further emission appears near 3450 cm^{-1} (figure 3). In addition to a no-phonon line at 3640 cm^{-1} several phonon-assisted transitions could be recorded. A sharp structure on the low-energy tail is generated by transitions of unintentionally incorporated Co^{2+} ions (Radliński 1979), as indicated in the figure. The analogue of the luminescence depicted in figure 3 for ZnSe is centred near 3750 cm^{-1} for ZnS:V and has tentatively been attributed to the $^5E(D) \rightarrow {}^5T_2(D)$ transition within a V^+ (d^4) centre. The V^+ ion is isoelectronic to Cr^{2+}, which is characterized by a triplet structure of the ground state (Vallin and Watkins 1974). Due to the low strength of the no-phonon line, no high-resolution measurements could be performed here. Therefore, information on a possible splitting of $^5T_2(D)$ cannot be derived for ZnSe:V. In recent measurements of the corresponding emission band in ZnS:V, however, the spin–orbit components of the ground state could be resolved (Goetz *et al* 1992).

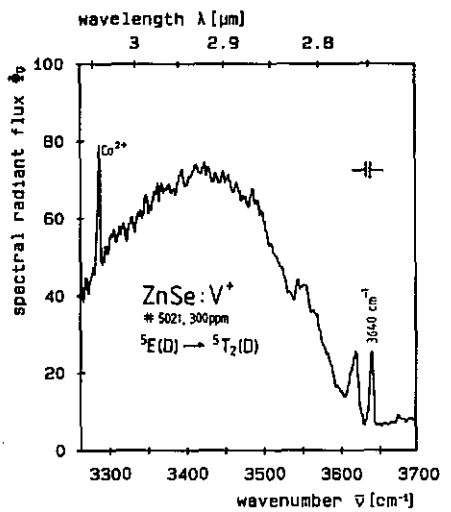

Figure 3. Emission spectrum of ZnSe:V^+ at $T \approx 4$ K (crystal number 5021); corrected spectrum. Excitation range: 9000 $cm^{-1} \leqslant \bar{\nu} \leqslant 14400$ cm^{-1}.

3. Excitation and absorption spectra

Excitation spectra were obtained by means of a double-prism spectrometer (Zeiss, MM12 with glass prisms). The radiant flux of the exciting radiation was kept constant by means of an automatic slit control. A high-pressure Xe lamp served as the light source. The radiation emitted from the crystals was selected by interference filters and detected by a cooled PbS cell.

The excitation spectra of the various V emissions in ZnSe which were presented in the previous section could be recorded separately for each charge state. The spectra

are largely in accordance with those of ZnS:V. For ZnSe, the spectral positions of the individual bands shift slightly towards smaller energies; their peak ratios, however, remain essentially the same. For both ZnS and ZnSe, the assignments of the excitation structures are based on model calculations for the excited states of V^{3+} and V^{2+}, as detailed in section 4.

The excitation spectrum of the V^{3+} emission (figure 4) is characterized by two excitation bands centred near 8890 cm^{-1} and 13 350 cm^{-1}, followed by a slow increase above 15 500 cm^{-1} merging into a strong excitation maximum at 22 400 cm^{-1}, i.e. near the band edge. The low-energy excitation band with a double peak at 8560 cm^{-1} and 8960 cm^{-1} is assigned to the $^3T_1(F) \leftarrow {}^3A_2(F)$ transition of the V^{3+} ion. Here the nomination of the $^3T_1(F)$ level and the (still to be discussed) $^3T_1(P)$ level follows the weak-field limit, as detailed in section 4. The 400 cm^{-1} splitting of the $^3T_1(F)$ level is ascribed to Jahn–Teller interaction in the excited state (Mircea-Roussel *et al* 1980, Biernacki *et al* 1988). It should be noted that this separation is much smaller than in ZnS, suggesting a weaker Jahn–Teller coupling in ZnSe also for the V^{3+} ion.

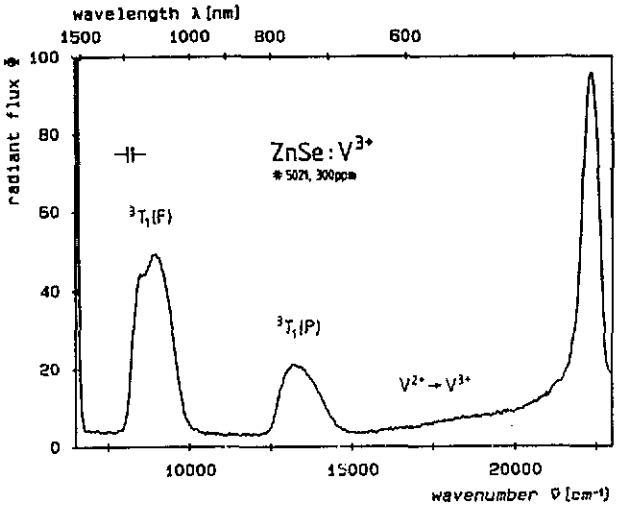

Figure 4. Excitation spectrum of the $^3T_2(F) \rightarrow {}^3A_2(F)$ luminescence of ZnSe:V^{3+} at $T \approx 4$ K (crystal number 5021). The emission is detected in the range: 5000 $cm^{-1} \leqslant \bar{\nu} \leqslant 6200$ cm^{-1}.

The weaker band at 13 350 cm^{-1} is attributed to the $^3T_1(P) \leftarrow {}^3A_2(F)$ transition, the triplet level with highest energy. It should be noted that no spin-forbidden transitions to singlet levels could be detected.

The slow increase of the V^{3+} excitation in the high-energy range above 15 000 cm^{-1} is assigned to a weak charge transfer band due to a change of the oxidation state $V^{2+} \rightarrow V^{3+}$ and will be discussed in section 5.

The excitation spectrum of the V^{2+} emission (figure 5), again, shows the same overall spectral features as in ZnS. In the low-energy range below 16 000 cm^{-1} a sequence of internal transitions is observed. The spectrum is dominated by two intensive bands centred near 8350 cm^{-1} and 10 220 cm^{-1}. In accordance with the assignments given for ZnS:V these bands are interpreted as the two spin-allowed transitions $^4T_1(P) \leftarrow {}^4T_1(F)$ and $^4A_2(F) \leftarrow {}^4T_1(F)$, respectively. The $^4T_1(P)$ state shows a twofold splitting with peaks at 8140 and 8560 cm^{-1}. As with ZnS:V, this

effect is explained by Jahn–Teller interactions, and just as in the case of the $^3T_1(F)$ level of the V^{3+} centre mentioned above, the coupling strength in ZnSe:V is much weaker than in ZnS:V.

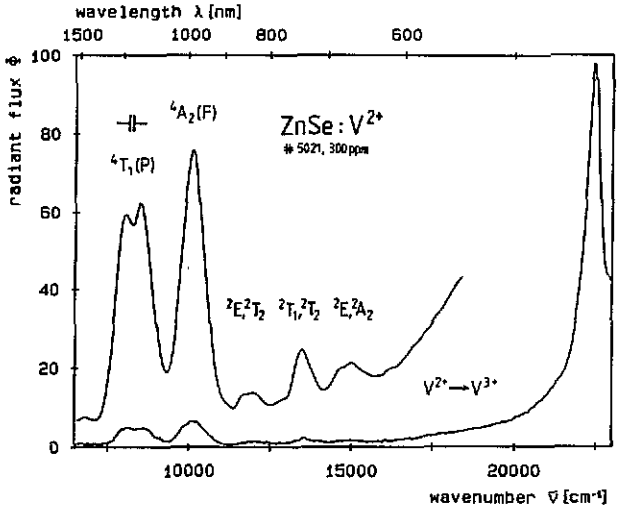

Figure 5. Excitation spectrum of the $^4T_2(F) \rightarrow {}^4T_1(F)$ luminscence of ZnSe:V^{2+} at $T \approx 4$ K (crystal number 5021). The emission is detected in the range: 3850 $cm^{-1} \leqslant \bar{\nu} \leqslant 4550$ cm^{-1}.

Several less intense excitation structures are assigned to spin-forbidden transitions from the $^4T_1(F)$ ground state to doublet levels originating from the ^2F, the lower energy ^2D, ^2H, ^2P and the ^2G terms of the V^{2+} ion. In table 1, the transition energies and assignments are compared with the computed values discussed in the next section.

Table 1. Transition energies for ZnSe:V given in cm^{-1}. For experimental values the centre of gravity of the corresponding transition band is listed.

	Exp.	Calc.	Assignment	Remark
V^{2+} (d^3)				
	16 200	17 057	$^2T_1(F)$	weak
	15 000	15 172; 15 401	$^2A_2(F)$; $^2E(D)$	fitted (C); doublet
$B = 264$	13 540	13 213; 13 502	$^2T_1(H)$; $^2T_2(F)$	fitted (C); shoulder
$C = 1322$	11 930	11 559; (12 409)	$^2E(H)$; ($^2T_2(D)$)	doublet
$\Delta = 5350$	10 220	10 220	$^4A_2(F)$	fitted (B, Δ)
	8350	8350	$^4T_1(P)$	fitted (B, Δ)
	6770	6915	$^2T_1(H)$	weak
	5110	4870	$^4T_2(F)$	cf text
V^{3+} (d^2)				
	13 350	13 486	$^3T_1(P)$	fitted (B, Δ)
$B = 304$	8890	8680	$^3T_1(F)$	fitted (B, Δ)
$\Delta = 5868$	5760	5868	$^3T_2(F)$	cf text

Following the internal crystal-field transitions, again a broad photo-ionization band rises near 15 000 cm^{-1} which is here more pronounced than in the V^{3+} spectrum.

In addition to the excitation measurements, sensitization spectra were recorded for the V^{3+} and V^{2+} emissions. The modulated principal excitation is provided by the light of a Xe lamp filtered out at an energy near 13350 cm^{-1}, where the V^{3+} emission as well as the V^{2+} emission are efficiently excited. Monochromatic light served as a continuously tunable unmodulated additional irradiation. Whereas 'red' auxiliary irradiation leads to an increase of the V^{3+} luminescence, it is quenched by 'green' light. Under the same experimental conditions, the V^{2+} luminescence reacts in an opposite manner (figure 6). The ratio $[V^{3+}]/[V^{2+}]$ of the concentrations of V centres with different oxidation states thus changes on scanning the additional irradiation. The threshold energy of 15500 cm^{-1} observed in the excitation spectra of V^{3+} and V^{2+} appears also in the sensitization spectra (cf section 5).

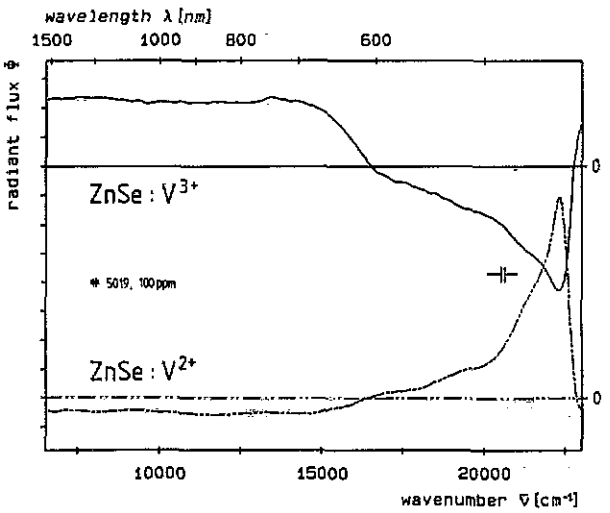

Figure 6. Sensitization spectra of the V^{3+} and V^{2+} luminescence at $T \approx 4$ K (crystal number 5019). The V^{3+} and V^{2+} bands are detected in the range of 5000 $cm^{-1} \leqslant \bar{\nu} \leqslant 6200$ cm^{-1} and 3850 $cm^{-1} \leqslant \bar{\nu} \leqslant 4550$ cm^{-1}, respectively. Both emissions are excited by $\bar{\nu} = (13350 \pm 200)$ cm^{-1}.

Distinct absorption bands could only be observed with a highly doped (3000 ppm) crystal. The spectra result from a superposition of several prominent V^{3+} and V^{2+} transitions. The most pronounced structures can be related to the low-energy edge of the $^4T_1(P) \leftarrow {}^4T_1(F)$ band of V^{2+}, to some further V^{2+} transitions known from the excitation spectra and to the $^3T_1(F) \leftarrow {}^3A_2(F)$ absorption of the V^{3+} centre. The simultaneous presence of both charge states presumably also determined earlier absorption measurements (Wray and Allen 1971, Le Manh and Baranowski 1977). In the higher-energy range, again a broad absorption sets in near 15500 cm^{-1} suggesting a charge transfer process (cf section 5).

4. Crystal-field calculations

The spectra presented in the previous sections are now analysed by crystal-field calculations based on the Tanabe–Sugano scheme (Tanabe and Sugano 1954). While more sophisticated models need additional parameters to account for polarization effects or

the influence of covalency, only three parameters (B, C and Δ) have to be adjusted to fit all multiplet levels of a given d^n configuration. This simple approximation gives a good description of the experimental values. For the computation, Griffith matrices (Griffith 1971) were used in the strong-field approximation and matrices given by Orgel (Orgel 1955) for the d^2 configuration and by Finkelstein and Van Vleck (1940) for the d^3 configuration in the weak-field regime.

Two similarities should be noted in the calculation of the V^{2+} (d^3) and V^{3+} (d^2) multiplets with the highest multiplicity which give rise to the strongest transitions. Firstly, in the T_d crystal-field both configurations have the same irreducible representations T_1, T_2 and A_2, originating from an F free-ion ground state. The ordering of ^4F crystal-field splitting of the d^3 configuration is, however, reversed with respect to the ^3F splitting of the d^2 configuration. Secondly, the corresponding crystal-field matrices contain only two parameters: the crystal-field splitting parameter Δ ($= 10$ Dq) and the Racah parameter B. Consequently, for the fit of all levels with other multiplicity only the Racah parameter C need be adjusted.

As no-phonon lines have not been detected in the excitation spectra, the barycentres of the excitation bands were utilized for fitting the energy positions of the crystal-field levels.

The two intense excitation bands of the V^{2+} (d^3) luminescence centred at 10 100 cm^{-1} and 8300 cm^{-1} are related to spin-allowed transitions from the $^4T_1(F)$ ground state to the quartet levels $^4A_2(F)$ and $^4T_1(P)$, respectively. The fit of the two experimental values by these excited d^3 levels yields $B = 264$ cm^{-1} and $C = 1322$ cm^{-1} (figure 7(*a*)). This procedure is checked by comparing the position of the luminescent $^4T_2(F)$ level resulting from the fit to that derived from the spectra. Since the $^4T_2(F) \leftarrow {}^4T_1(F)$ excitation band could not be measured directly, its peak position is estimated by adding the energy difference between the emission band maximum and the no-phonon lines to the average energy of the NPL. This evaluation assumes a symmetrical Franck–Condon shift in the vibronic relaxation. As shown in figure 7(*a*), the energy determined in this way is close to the calculated value (table 1).

The weak excitation structures above the $^4A_2(F)$ band are attributed to the spin-forbidden transitions to doublet levels (cf table 1). The corresponding energy matrices, in addition, contain the Racah parameter C. For its determination, B and Δ were kept constant and the excitation bands centred near 15 000 cm^{-1} and 13 540 cm^{-1} were fitted by $^2E(D)$, $^2A_2(F)$ and $^2T_1(H)$, $^2T_2(F)$, respectively. This calculation results in a good approximation of all observed excitation structures. The assignment of the levels $^2\Gamma_i$ to their free-ion term origin ^2L (at $\Delta = 0$) given in table 1 reflects the strongest contribution determined in weak-field calculations. Especially the $^2T_1$ levels originating from the ^2P and ^2H term are strongly mixed due to the degeneracy of the two free-ion terms.

It should be noted that, for the B and C values obtained, the ground state changes from the high-spin $^4T_1(F)$ level to the low-spin $^2E(G)$ level when Δ exceeds 6080 cm^{-1}. Beyond this point an amount of approximately 0.98 cm^{-1} for an increase of Δ by 1 cm^{-1} has to be added to the energies read from figure 7(*a*) in order to refer to the low-spin ground state.

For the approximation of the V^{3+} (d^2) energy levels, a procedure similar to that described above has been applied yielding $B = 304$ cm^{-1} and $\Delta = 5868$ cm^{-1}. The two excitation bands (cf figure 4) are assigned to transitions to the levels $^3T_1(P)$ and $^3T_1(F)$ (figure 7(*b*)). Calculations within the weak-field scheme reveal an 8%

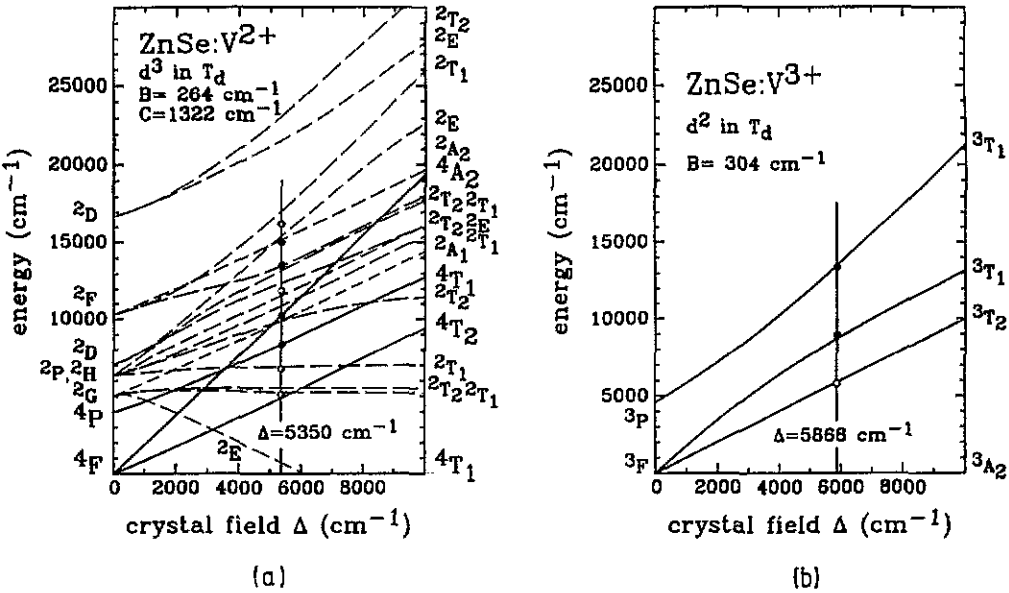

Figure 7. Crystal-field level splitting of V^{2+} (d^3), (LHS), and V^{3+} (d^2), (RHS) calculated following the Tanabe–Sugano scheme. Circles indicate empirical transition energies; those marked by closed circles have been used to derive the parameters B, C and Δ. In the left diagram, all energies are referred to the $^4T_1(F)$ high-spin ground state, for a better view even above $\Delta = 6080$ cm^{-1} (see text). The vertical line denotes the fitted crystal-field parameter Δ.

admixture of the ^3P term to the $^3T_1(F)$ level at the determined crystal-field Δ and *vice versa* for $^3T_1(P)$.

Again the position of the luminescent $^3T_2(F)$ level is well described by B and Δ determined from the fit of the two $^3T_1$ levels (cf table 1). The Racah parameter C could not be deduced, as no additional structures representing V^{3+} transitions to singlet levels have been found.

Comparing the parameters B and Δ which describe the two charge states of the V ion considered, an increase is found on passing from V^{2+} (d^3) to V^{3+} (d^2) (15% and 10%, respectively). A comparable situation is observed with ZnS; this leads essentially to a simple scaling up of B and Δ by the same factors. For a given configuration, B, Δ and all transition energies increase by roughly 7% when the host crystal ZnSe is replaced by ZnS. The crystal-field scheme thus gives a coherent description of vanadium in both these materials.

5. Charge transfer processes at vanadium centres in ZnSe

By excitation in suitable spectral regions, a reversible conversion of the individual charge states is attained (cf section 3). From the excitation, transmission and sensitization spectra, two energies are derived:

(i) an edge at 15 500 cm^{-1}, which appears in the transmission as well as in the excitation spectra of the V^{3+} emission (cf figure 4) and V^{2+} emission (cf figure 5);

(ii) a threshold near 12 000 cm^{-1} in the excitation spectrum of the V^+ emission (the V^+ centre and the related spectra will be discussed in more detail in a separate

paper (Goetz *et al* 1992)).

Further information is obtained from the sensitization experiments (cf figure 6):

(iii) the measurements with 'red' additional irradiation lead to an increase of the V^{3+} signal and simultaneously to a decrease of the V^{2+} luminescence;

(iv) sensitization with 'green' additional irradiation stimulates the V^{2+} emission and quenches the V^{3+} luminescence at the same time.

In both these optical biasing spectra, a reversal starts near 15 500 cm^{-1}. The stated transition energies cannot be connected to crystal-field transitions characteristic of one particular charge state of vanadium. They are most probably related to charge-transfer processes involving V and band states of the host crystal. In the following, the transitions are discussed on the basis of a simple charge-transfer model of an amphoteric defect. A more detailed consideration will follow in a later publication.

The energy of the vanadium donor has already been determined by electrical methods, namely 16 100 cm^{-1} below the edge of the conduction band (Dieleman 1967). Theoretical predictions for the position of the donor level vary considerably: the distance to the minimum of the conduction band is given as 4950 (Tian and Shen 1989), 6450 (Baranowski and Vogl 1983), 7300 (Kikoin *et al* 1990), or 10 800 cm^{-1} (Vogl and Baranowski 1983). For the acceptor transition, the energy of 16 900 cm^{-1} with respect to the valence band was calculated (Vogl and Baranowski 1983).

Following those theoretical studies which place the V^{2+}/V^{3+} donor level in the upper part of the band gap, the threshold found in the V^{2+} and V^{3+} excitation spectra at 15 500 cm^{-1} could describe the photoneutralization: $V^{3+} + 15\,500\ cm^{-1} \rightarrow V^{2+} + e^{+}_{VB}$ (e^{+}_{VB}: hole in the valence band). This assignment would place the V^{2+} donor level so high in the band gap that the higher crystal-field levels of V^{2+} would be degenerate with the conduction band—in contradiction to the experimental results which prove that excitation to crystal-field levels at energies up to 15 000 cm^{-1} still entails the V^{2+} emission (cf figure 5 and table 1). Therefore the threshold energy is connected with the donor process proper:

$$V^{2+} + 15\,500\ cm^{-1} \rightarrow V^{3+} + e^{-}_{CB}. \tag{1}$$

This photo-ionization energy is in good agreement with the value of 16 100 cm^{-1} (Dieleman 1967) determined by means of electrical methods but deviates decidedly from the calculated values given above.

To account for the internal V^{3+} and V^{2+} emission processes, vanadium must attain the excited states V^{3+*} and V^{2+*}. This will be shown below to result from hole capture by V^{2+} and V^{+}, respectively, after acceptor-type transitions (cf reaction (4)). The following sequences of different relaxation processes are then conceivable. On the one hand, the excited V^{3+*} ion can at first emit the spectrum characteristic for the d^2 configuration (V^{3+} luminescence):

$$V^{3+*} \rightarrow V^{3+} + 5400\ cm^{-1}. \tag{2}$$

On the other hand, capture of a free electron (created by process (1)) generates an excited V^{2+*} ion, giving rise to the V^{2+} emission:

$$V^{3+*} + e^{-}_{CB} \rightarrow V^{2+*} \rightarrow V^{2+} + 4700\ cm^{-1}. \tag{3}$$

Emission measurements substantiate that under broad-band excitation ($16\,500\ cm^{-1} \leqslant \bar{\nu} \leqslant 27\,000\ cm^{-1}$) the V^{2+} emission is favoured above the V^{3+} emission. This is also reflected in the excitation spectra.

In the sensitization experiments, V^{3+} has been excited through $^3T_1(P)$ and V^{2+} via the levels $^2T_1(H)$ and $^2T_2(F)$ (cf table 1). Both emissions could therefore be detected simultaneously. The complementary luminescence behaviour under additional irradiation (cf figure 6) shows that 'red' light leads to a charge transfer $V^{2+} \rightarrow V^{3+}$ and 'green' light to the reverse reaction. Obviously two different processes occur, the one opened by 'green' light being more efficient. These results can be explained by participation of unknown centres generating free carriers under the influence of the adjunct unmodulated light.

Under irradiation by 'red' unmodulated light, at first a transition from the valence band to the unknown centre takes place, generating holes in the valence band. The free holes can be trapped by V^{2+} ions, so that V^{3+} centres ensue: $e^+_{VB} + V^{2+} \rightarrow V^{3+}$. Consequently, the ratio $[V^{2+}]/[V^{3+}]$ of the concentrations will change in favour of V^{3+}. The V^{3+} centres generated in this manner can then be excited by modulated light via an internal transition, thus entailing an increase of the V^{3+} emission. The described process also explains quenching of the V^{2+} emission by 'red' additional irradiation.

Under the influence of 'green' additional irradiation, transitions from the unknown centre to the conduction band are induced; the liberated electrons can recombine with V^{3+} to V^{2+} centres: $e^-_{CB} + V^{3+} \rightarrow V^{2+}$. The number of V^{2+} centres and the corresponding emission are thus increased, accompanied by an attenuation of the V^{3+} luminescence.

The unknown defect assumed in these deliberations is probably the self-activated (SA) centre (Lee *et al* 1980, Schrittenlacher *et al* 1984). All ZnSe:V specimens under study show a broad luminescence band peaking near $16\,000\ cm^{-1}$ which is attributed to this zinc-vacancy/donor complex.

The threshold energy of $12\,000\ cm^{-1}$, derived from the excitation spectrum of the V^+ emission (Goetz *et al* 1992) is related to an acceptor-type transition

$$V^{2+} + 12\,000\,cm^{-1} \rightarrow V^+ + e^+_{VB}. \tag{4}$$

This threshold energy being smaller than that of the donor-type process (1) above, generation of free holes must be considered additionally under the conditions of excitation at $\bar{\nu} \geqslant 15\,500\ cm^{-1}$. The free holes thus generated can be captured by V^+ and V^{2+} centres:

$$V^+ + e^+_{VB} \rightarrow (V^{2+})^* \tag{5a}$$

and

$$V^{2+} + e^+_{VB} \rightarrow (V^{3+})^*. \tag{5b}$$

While intraconfigurational transitions dominate the spectra between 12 000 and $15\,500\ cm^{-1}$ (cf figures 4 and 5), the reactions (5*a*) and (5*b*) become important at higher energies.

Process (4) would place the vanadium acceptor near the middle of the gap. In principle, the complementary transition should be possible as well:

$$V^+ + 12\,000\,cm^{-1} \rightarrow V^{2+} + e^-_{CB}. \tag{6}$$

Which of the transitions (4) or (6) occurs can only be decided if the sign of the generated charge carriers is known. Reaction (4) seems to be preferred because of the anticipated prevalence of the quasi-neutral V^{2+} oxidation state. To resume, also in the case of the acceptor, the experimental value (cf reaction (4)) deviates strongly from the position of 16 900 cm^{-1} deduced theoretically (Vogl and Baranowski 1983).

The results presented in this section suggest that the ground-state levels of the three vanadium oxidation states V^{3+}, V^{2+} and V^{+} are located in the lower half of the band gap, i.e. below the V^{2+}/V^{+} acceptor level defined by reaction (4). The minimum energies required for the conversion of the individual charge states are comparatively low so that the co-appearance of the three described charge states of vanadium becomes comprehensible.

6. Conclusions

The presented optical emission and excitation spectra of V-doped ZnSe crystals arise from internal electronic transitions assigned to V^{3+}, V^{2+}, and tentatively to V^{+} ions. The V^{3+} and the V^{2+} ions are subject to dynamic Jahn–Teller interactions. This effect is evidenced in the fine-structure of the emission as well as in the excitation spectra of the corresponding configuration. The coupling strength, however, is weaker in ZnSe than in ZnS. For the V^{2+} centre this is indicated by a sixfold splitting of the no-phonon transition $^4T_2(F) \rightarrow {}^4T_1(F)$ and the splitting within the excited $^4T_1(P)$ state. For the V^{3+} centre the same trend is confirmed by the analogous splitting of the $^3T_1(F)$ state.

Whereas for V^{2+} distinct spin-forbidden quartet–doublet transitions appear in both the ZnSe and ZnS excitation spectra, for the V^{3+} centre no triplet–singlet transitions could be detected.

The excitation spectra of the V^{3+} (d^2) and V^{2+} (d^3) luminescence are well described by calculations which are based on the Tanabe–Sugano scheme. Comparison with results for ZnS:V shows that all transition energies of V^{2+} and V^{3+} are approximately 7% smaller in ZnSe than in ZnS. Consequently the parameters B and Δ of the crystal-field calculations are scaled down by this amount.

Three different oxidation states of the V centre appear simultaneously. Moreover, two charge transfer transitions $V^{3+} + e^{-}_{CB} \rightleftarrows V^{2+}$ and $V^{2+} \rightleftarrows V^{+} + e^{+}_{VB}$ between these states were achieved optically. The balance between V^{3+} and V^{2+} is also influenced directly in sensitization experiments.

Acknowledgments

We are grateful to S W Biernacki, J Dreyhsig and B Litzenburger for useful discussions in the crystal-field model calculations and to M Thiede for skilful technical assistance. One of the authors, GG, gratefully acknowledges the stipend of the Max-Planck-Gesellschaft.

References

Allen J W 1963 *Physica* 29 764–8

Armelles J, Barrau J, Thébault D and Brousseau M 1984 J. Physique **45** *1795–800*
Aszódi G and Kaufmann U 1985 *Phys. Rev.* B **32** 7108–15
Avinor M and Meijer G 1960 *J. Phys. Chem. Solids* **12** 211–15
Baranowski J M and Vogl P 1983 *12th Conf. Physics of Semiconducting Compounds (Jaszowiec) (Proc. Conf. Phys. 6)* pp 74–96
Biernacki S W, Roussos G and Schulz H-J 1988 *J. Phys. C: Solid State Phys.* **21** 5615–30
Buhmann D, Schulz H-J and Thiede M 1979 Phys. Rev. B **19** 5360–8
Caldas M J, Figueiredo S K and Fazzio A 1986 *Phys. Rev.* B **33** 7102–9
Dieleman J 1967 *II-VI Semiconducting Compounds* ed D G Thomas (New York: Benjamin) pp 199–206
Finkelstein R and van Vleck J H 1940 *J. Chem. Phys.* **8** 790–7
Goetz G, Pohl U W, Schulz H-J and Thiede M 1992 *Verhandl. DPG* (VI) **27** HL 7.68
Goetz G and Schulz H-J 1992 unpublished
Griffith J S 1971 *The Theory of Transition Metal Ions* 3rd edn (Cambridge: Cambridge University Press)
Hennel A M, Brandt C D, Ko K Y, Lagowski J and Gatos H C 1987 *J. Appl. Phys.* **62** 163–70
Irwin J C and LaCombe J 1972 *Can. J. Phys.* **50** 2596–604
Katayama-Yoshida H and Zunger A 1986 *Phys. Rev.* B **33** 2961–4
Kikoin K A, Kurek I G and Mel'nichuk 1990 *Sov. Phys.–Semicond.* **24** 371–2
Koidl P 1976 *Phys. Status Solidi* b **74** 477–84
Lee K M, Dang L S and Watkins G D 1980 *Solid State Commun.* **35** 527–30
Le Manh H and Baranowski J M 1977 *Phys. Status Solidi* b **84** 361–5
Meijer G and Avinor M 1960 *Philips Res. Rep.* **15** 225–37
Mircea-Roussel A, Martin G M and Lowther J E 1980 *Solid State Commun.* **36** 171–3
Mitra S S 1966 *J. Phys. Soc. Japan* **21** 61–6
Nash K J, Skolnick M S, Cockayne B and MacEwan W R 1984 *J. Phys. C: Solid State Phys.* **17** 6199–209
Orgel L E 1955 *J. Chem. Phys.* **23** 1004–14
Pohl U W, Ostermeier A, Busse W and Gumlich H-E 1990 *Phys. Rev.* B **42** 5751–8
Radliński A P 1979 *J. Lumin.* **18/19** 147–50
Schrittenlacher W, Nelkowski H and Pradella H 1984 *Phys. Status Solidi* b **122** 285–94
Schulz H-J, Roussos G and Biernacki S W 1990 *Z. Naturf.* a **45** 669–76
Skolnick M S, Dean P J, Kane M J, Uihlein Ch, Robbins D J, Hayes W, Cockayne B and MacEwan W R 1983 *J. Phys. C: Solid State Phys.* **16** L767–75
Tanabe Y and Sugano S 1954 J. Phys. Soc. Japan **9** 753–79
Tian Z and Shen X 1989 *J. Appl. Phys.* **66** 2414–19
Vallin J T and Watkins G D 1974 *Phys. Rev.* B **9** 2051–72
Vogl P and Baranowski J M 1983 unpublished
Wray E M and Allen J W 1971 *J. Phys. C: Solid State Phys.* **4** 512–16